Photonuclear cross sections for ^{18}O

J. G. Woodworth, K. G. McNeill,* J. W. Jury,† R. A. Alvarez, B. L. Berman, D. D. Faul, and P. Meyer
Lawrence Livermore Laboratory, University of California, Livermore, California 94550
(Received 24 July 1978; revised manuscript received 27 November 1978)

All the major photonuclear cross sections for ^{18}O, including $\sigma(\gamma,p)$, $\sigma[(\gamma,n)+(\gamma,np)]$, and $\sigma(\gamma,2n)$, were measured as a function of photon energy from threshold to 42 MeV. The photon energy resolution was between 200 and 300 keV. The source of radiation was the monoenergetic photon beam obtained from the annihilation in flight of fast positrons. The partial photoneutron cross sections were determined by neutron multiplicity counting, and the average neutron energies for both single- and double-photoneutron events were determined simultaneously with the cross-section data by the ring-ratio technique. The photoproton cross section was determined by counting the delayed neutrons from the β-decay of the residual ^{17}N nuclei. Integrated cross sections were extracted from the data and compared with sum-rule predictions. Resonances in the pygmy-resonance region exhibit substantial decay branching to negative-parity states in ^{17}O. Significant differences in the branching of resonances in the giant-resonance region to the various partial cross sections, together with the photoneutron-energy data, allow isospin assignments to be made for all the resonances, with the consequent delineation of the isospin strength distribution for ^{18}O. Evidence was found for two weak but broad resonances above the giant-resonance region. Finally, comparison with the corresponding cross sections for ^{16}O shows considerable differences between the two nuclei.

[NUCLEAR REACTIONS $^{18}O(\gamma,n)$, E_γ=8.0–41.8 MeV; measured 4π prompt, delayed neutron yield for monoenergetic photons; $\sigma(E_\gamma,1n)$, $\sigma(E_\gamma,2n)$, $\sigma(E_\gamma,p)$, integrated cross sections; detailed distribution of isospin strength; comparison with ^{16}O.]

I. INTRODUCTION

This paper is one of a series reporting on a collaborative effort to study in detail the nuclear photoeffect in light nuclei having one or two nucleons outside closed (4N) shells. Another paper in this series[1] reports on the total and partial photoneutron cross sections for ^{13}C, and a third paper[2] describes a measurement of the differential ground-state photoneutron cross section for ^{17}O.

The present paper reports on the simultaneous measurement of all of the major photonuclear cross sections for ^{18}O, namely, the $(\gamma,1n)$ $=[(\gamma,n)+(\gamma,np)]$, the $(\gamma,2n)$, and the (γ,p) reactions. The measurements were made with monoenergetic photons obtained from the annihilation in flight of fast positrons at the Lawrence Livermore Laboratory Electron-Positron Linear Accelerator facility.

The threshold energies for photonuclear reactions on ^{18}O are given in Table I. The ^{18}O nucleus is *unique* among stable nuclei in that its (γ,p) threshold (15.94 MeV) lies *higher* in energy than its $(\gamma,2n)$ threshold (12.19 MeV) (Ref. 3); this means that the residual nucleus from the ^{18}O (γ,p) process, namely ^{17}N, can decay by β^- emission to neutron-unstable states in ^{17}O. Therefore, the ^{18}O (γ,p) cross section can be measured by observing the resulting delayed neutrons, while the prompt photoneutrons yield the (γ,n) and $(\gamma,2n)$ cross sections in the usual way. Figure 1 illustrates the reaction channels measured in this experiment. This is the first time that all the major photoreaction channels for a light nucleus have been measured independently with monoenergetic photons using the same beam, the same sample, and the same detector. This simultaneous detection of both the photoproton and photoneutron events permits comparison of these cross sections with a high level of confidence; and the fact that all the major channels are accounted for makes possible the determination of the total photon absorption cross section for a light nucleus free from most of the uncertainties which arise when summing the results of the separate partial cross sections which frequently have been measured at different laboratories.

The photoabsorption cross section for ^{18}O can be divided conveniently into three energy regions: (1) the region below the giant dipole resonance (GDR), up to about 17 MeV, sometimes called the region of the pygmy resonance, (2) the region of the GDR, from about 17 to 31 MeV, and (3) the region above the GDR.

The pygmy resonance for ^{18}O is expected to be made up of a number of strong and distinct resonances, rather than a more or less continuous distribution of strength with relatively weak resonances superposed, as is the case for ^{13}C (Ref. 1). This is attributed to the fact that only 1^- states

TABLE I. Threshold energies for ^{18}O (from Ref. 3).

Reaction	Threshold energy (MeV)
$^{18}O(\gamma,\alpha)$	6.228
$^{18}O(\gamma,n)$	8.045
$^{18}O(\gamma,2n)$	12.189
$^{18}O(\gamma,\alpha n)$	14.404
$^{18}O(\gamma,p)$	15.942
$^{18}O(\gamma,np)$	21.825
$^{18}O(\gamma,3n)$	27.853

are excited by $E1$ transitions from the ground state of an even-even nucleus like ^{18}O, while several spin states (and consequently a much denser and perhaps overlapping distribution of resonances) are excited by $E1$ transitions in an odd-A nucleus. The GDR for ^{18}O is expected to be dominated by a few strong resonances, rather than a continuous distribution, again as is appropriate for an even-even nucleus. It is instructive to examine in this regard the magnesium isotopes (Ref. 4), where this behavior appears in extreme form.

Early measurements of the photoreactions for ^{18}O, all of which were performed with continuous bremsstrahlung radiation sources, observed individually prompt photoneutrons,[5,6] delayed neutrons,[7-9] or photoprotons,[10,11] but none of these early efforts produced the kind of detail necessary to compare with the present work. Also, the only electron-scattering measurement[12] in an overlapping energy region was done at 180°, which selectively excites only magnetic transitions.

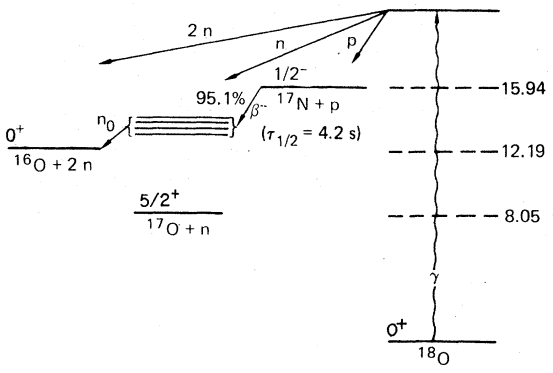

FIG. 1. The main particle-decay channels for ^{18}O, with their separation energies (in MeV). Note that the proton separation threshold lies above that for two-neutron emission—a feature unique among stable nuclei—permitting β^- decay from ^{17}N to neutron-unbound states in ^{17}O, which occurs 95.1% of the time.

Recently, however, two more detailed photoneutron measurements on ^{18}O have been made: Allan *et al.*[13] measured the ground- and first-excited-state cross sections in the pygmy-resonance region (from 10 to 18 MeV) by the neutron-time-of-flight technique, and Kneissel *et al.*[14] measured the (γ,n) and $(\gamma,2n)$ cross sections up to 33 MeV with monoenergetic photons. The present measurement of the total, integrated-over-angle, photoneutron cross section complements that of Ref. 13 of the differential, 98°, partial cross sections, thus giving further information on the character of the sharp resonances in the pygmy region. To the results of Ref. 14, the present work adds information on the average energy of the emitted photoneutrons and extends the region of coverage up to ~42 MeV. Also, certain important discrepancies between the present results and those of Ref. 14 will be noted below.

Although no detailed theoretical calculation for the distribution of dipole strength specific to ^{18}O yet has been reported, comparison of the present experimental results with several general theories still can be made. The ground-state isospin of ^{18}O is $T_0 = (N-Z)/2 = 1$. Since ^{18}O is not a self-conjugate nucleus, both $T_< = T_0 = 1$ and $T_> = T_0 + 1 = 2$ components of the GDR can be excited via photoabsorption. Since both the photoproton and photoneutron cross sections are measured in the present experiment, and since the average photoneutron energies are determined as well, it is possible, with some assumptions, to separate the two isospin components across the region of the GDR (and below).

Comparison of the photodisintegration cross sections for ^{18}O with those for ^{16}O also might be interesting. Similar features in the cross sections might be expected if the model of the ^{18}O nucleus as consisting of an ^{16}O core plus two valence neutrons is essentially correct and if the ^{16}O core is perturbed only slightly by the presence of the valence neutrons (see Ref. 15).

II. EXPERIMENTAL METHOD

The same basic method has been used in performing the present experiment as has been used in the past, although a number of changes have been made as the photonuclear program at Lawrence Livermore Laboratory has matured and evolved. These include the design and position of the positron source and certain beam-transport components, and more important, the revision and modernization of the data-reduction programs and procedures: They now are in modular form (and follow upon each other in logical sequence) so that

the data can be examined at any stage in the analysis, and human interaction with the computer programs is not only possible, but is used routinely where such interaction is desirable. Previous accounts which include considerable descriptive material have been published in Refs. 16–21; Refs. 19–21, particularly the review article by Berman and Fultz (Ref. 21), contain material on techniques used at other laboratories as well. An updated description of the Livermore annihilation-photon facility and methods is given in Ref. 22.

The measurements reported here were performed using the Lawrence Livermore Laboratory Electron-Positron Linear Accelerator at beam-pulse rates up to 1440 Hz. Positrons created by pair production in a W-Re converter were passed through a series of bending and focusing magnets and an energy-analyzing slit. During runs with electrons the fields of the magnets were reversed and electron currents comparable to those obtained with positrons (~1 or 2 nA) were collected from the converter. The beam was passed through a 12.7-mm-diameter beryllium annihilation target; after passing through the target the remaining beam was deflected magnetically into a 5-m-deep dump well in the floor. Negligible background was produced from the sides of the well.

The collimated photon beam passed through a spherical xenon-filled transmission ionization chamber onto the sample. The stability and calibration of the ion chamber was monitored by placing a ^{60}Co source into a standard position near the ion chamber periodically during the course of the experiment.

The sample was located in the center of the 4π neutron detector. A remotely controlled eight-position sample changer enabled any of seven samples or a standard neutron calibration source to be placed pneumatically into this position.

Verification of the energy scale and resolution was obtained from the observed position and width of the narrow 15.11-MeV resonance in ^{13}C (its natural width is about 5 keV). This was seen to set an upper limit of 240 keV on the resolution at this energy.

The neutron detector consists of a 61-cm cube of paraffin in which 48 high-pressure BF_3 tubes have been placed in four concentric rings of twelve tubes each. Signals from each of the four rings were gated by two separate gates. The prompt gate began 4.5 μs after the beam pulse and was 300 μs wide. The delayed gate settings varied according to the repetition rate of the accelerator. Since the more energetic photoneutrons from the sample travel farther through the paraffin before being thermalized, relatively more fast neutrons will be detected in the outermost ring than slow ones. Consequently, the ratio of the counting rate in the outer ring to that in the inner ring increases monotonically with neutron energy.

The absolute ring-ratio and efficiency scales were fixed by using a variety of distributed and monoenergetic neutron sources. A Monte Carlo neutron-transport code[23] also has been used in order to complement the experimental studies. During the experimental runs the absolute scale for these curves was monitored using a standard Pu-Be neutron source.

Changes in the efficiency and ring-ratio curves for the neutron detector occurred when it held hydrogenous samples such as the isotopically enriched $H_2\,^{18}O$, since they introduced more moderating material. The Monte Carlo neutron-transport code was used to compare the effect of different sized water samples with the normal efficiency at different neutron energies and to make appropriate corrections. The calculated curves for a 120-g water sample were checked experimentally by running hydrogenous samples of different sizes at the same photon energy.

The neutron yield data were subject to four types of background contamination which were measured carefully and subtracted from the data:

(i) Machine-off background counts resulted from cosmic rays. The magnitude of this background was typically less than 1% of the true counts, at all but the lowest energies, and its subtraction introduced negligible uncertainty.

(ii) Neutron backgrounds measured with the annihilation target removed, but the machine on, varied from essentially zero at low positron energies to about 2% of the true neutron events at the highest energy. These were measured at each energy and introduced negligible uncertainty.

(iii) The beam-dependent, sample-out neutron background also was measured and subtracted from the data. This was at most a 10% effect and was accounted for with negligible uncertainty.

(iv) The neutron background from the empty sample holder was determined from measurements using an empty lucite container of similar dimensions and mass to the containers holding the samples. The relative magnitude of this background varied with the different samples, but the maximum background was about 30%.

The photoproton reaction in ^{18}O yields the product nucleus ^{17}N, which decays by β^- emission with a half-life of 4.174 s to excited states in ^{17}O. The ^{17}O nucleus is left in neutron-unbound excited states 95.1% of the time, and so decays predominantly by neutron emission. The ^{18}O (γ, p) cross section was determined by measuring the yield of these delayed neutrons. The average delayed-neutron energy was measured by using the measured

TABLE II. Sample characteristics.

Sample	Composition (at. %)	Net mass (g)	Sample-blank mass (g)	l (g/cm^2)
^{18}O (large)	^{16}O- 1.58 ^{17}O- 1.92 ^{18}O-96.5	118.55	28.35	10.139
^{18}O (small)	^{16}O- 1.6 ^{17}O- 1.8 ^{18}O-96.6	34.7	19.75	2.70
^{17}O[a]	^{16}O-10.4 ^{17}O-20.3 ^{18}O-69.3	101.60	38.78	8.215

[a]Delayed neutrons from this sample aided in determining the ^{18}O(γ,p) cross section.

ring ratios and found to agree with the value derived from Ref. 24.

The data reported here were obtained during two separate experiments. Table II shows the details for each sample.

D_2O and H_2O samples also were run at several energies. These served to check the experimental accuracy, since the absolute cross sections of deuterium and oxygen have been studied and are well known. The deuterium sample also was used to evaluate the prompt contamination of the delayed neutrons.

III. DATA REDUCTION

The following describes the procedures by which the data were reduced to cross sections, in the order in which they were applied to the data. They are described in detail in Ref. 22.

(a) *Pile-up correction.* Even though counting rates were kept low enough (<1%) to minimize appreciable pile-up of counts in the detector [e.g., two $(\gamma, 1n)$ events appearing as an event from the $(\gamma, 2n)$ reaction], a correction was made for this statistical effect. The uncertainty in this correction is negligible.

(b) *Removal of annihilation-target-out background.* Actual or interpolated values of neutron and ion-chamber backgrounds were subtracted from the data for both the positron and electron measurements. Neutron backgrounds typically necessitated about a 1% correction and resulted mainly from the cosmic-ray background. Ion-chamber backgrounds typically necessitated about a 10% correction (which, however, was determined very precisely).

(c) *Drift of the neutron detector and ion chamber.* Measurements of the response of the neutron detector and ion chamber were made at frequent intervals during the experiment using standard neutron and γ-ray calibration sources. The largest deviations from the average responses were less than 2%, and were taken into account in the data reduction, with negligible resultant uncertainty.

(d) *Delayed-neutron background.* For samples containing the ^{18}O isotope, a steady background of delayed neutrons contaminated the prompt neutron counts in the energy region where the ^{18}O (γ, p) cross section was significant. The effect of this contamination was accounted for with negligible uncertainty.

(e) *Subtraction of the yields from positron bremsstrahlung.* Measured or interpolated reaction counts for the runs using electrons were normalized to equal ion-chamber readings and subtracted at each energy from the corresponding counts measured using positrons. Uncertainties arising from the subtraction procedure are negligible, except perhaps at the very highest energies measured.

(f) *Subtraction of sample-blank background.* Each sample was contained in a hollow 38.1-mm diameter right circular cylinder of Lucite $(H_8C_5O_2)$ held in a standardized Styrofoam rabbit for use in the pneumatic sample changer. The background from the sample holder plus other sources was measured and accounted for, with $\lesssim$2% uncertainty.

(g) *Conversion of ring ratios to efficiencies.* The efficiencies for detecting neutrons of a given multiplicity can be determined from the ratio of counts in the outer to those in the inner ring of the neutron detector. The uncertainty in the efficiencies so determined varies from about 2% at low neutron energies to about 10% at the highest neutron energies encountered in this experiment. The ring ratio for each neutron multiplicity can be converted to give a measure of the average neutron energy, thus providing a valuable measure of the residual excitation energy of the daughter nucleus.

(h) *Photon attenuation in the sample.* The photon

beam is reduced in intensity during its passage through the sample; the correction for this is $G = \mu l/(1 - e^{-\mu l})$, where μ is the photon mass attenuation coefficient for the sample and l is its thickness. This factor G is energy dependent; the required variations of μ with energy are given in Ref. 25. The values of l in g/cm^2 for each sample are given in Table II. The uncertainty arising from this correction is negligible.

(i) *Conversion to cross sections.* The $(\gamma, 1n)$ and $(\gamma, 2n)$ net yield data were converted to photoneutron cross sections by applying the separately measured calibration of the ion-chamber response per annihilation photon, the known number of ^{18}O nuclei in the photon beam, and the ratio of solid angles subtended by the ion chamber and the sample. The uncertainty in the photon-flux calibration is about 6% below 30 MeV and slightly larger at higher energies.

(j) *Evaluation of the ^{18}O (γ,p) ^{17}N cross section.* For samples containing ^{18}O, the total number of delayed neutrons per unit ion-chamber response, having been corrected for prompt neutrons with the use of Eq. (4), can be used to evaluate the ^{18}O (γ, p) cross section. Since the ^{17}O sample (as well as the ^{18}O samples) contained a substantial amount of ^{18}O, three sets of data were available for this purpose.

No pileup or multiplicity corrections were necessary for the delayed-neutron data; thus immediately after subtraction of the bremsstrahlung component, these data could be used to obtain the ^{18}O (γ, p) cross section. (Since the delayed neutrons result from the β^- decay of ^{17}N, the branching ratio and energy distribution of these neutrons are known.[24])

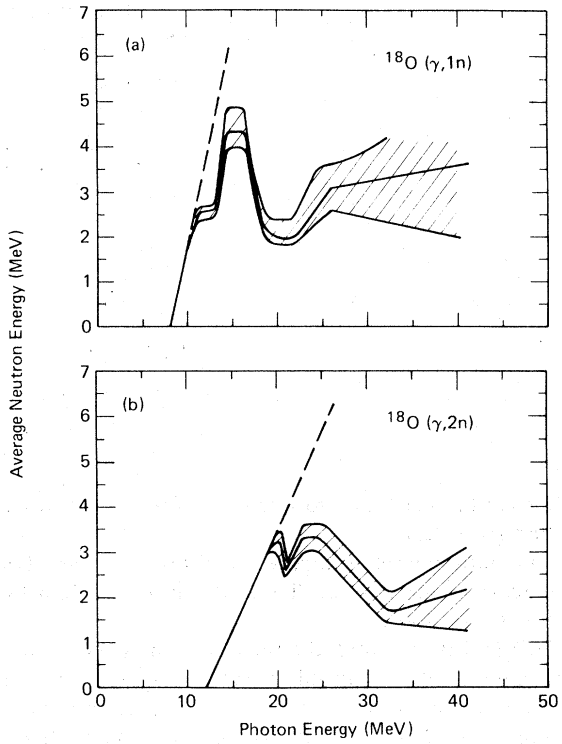

FIG. 2. The average emitted neutron energy versus photon energy for the (a) $^{18}O(\gamma, n)$ and (b) $^{18}O(\gamma, 2n)$ reactions. The shaded bands reflect statistical uncertainty of the measured data points. The straight dashed lines show the neutron energy expected if all decays populated the ground state of the daughter ^{17}O or ^{16}O nucleus.

IV. RESULTS

A. Average neutron energies

Plots of the average neutron energy, derived from the ring-ratio data, are shown in Fig. 2; Fig. 2(a) shows the average neutron energy for single-photoneutron reactions [which might include (γ, np) as well as (γ, n) events], and Fig. 2(b) shows this quantity for neutrons from the $(\gamma, 2n)$ reaction. The dashed lines in these plots represent the maximum possible neutron energies, which would be observed if all transitions proceeded to the ground states of the residual nuclei.

The average neutron energy for single photoneutrons [Fig. 2(a)] rises rapidly from the (γ, n) threshold, through a shoulder located from 11 to 12.5 MeV photon energy, to a maximum of about 4.3 MeV located from 14.5 to 16 MeV. An abrupt decrease then occurs between 16.5 and 18 MeV to a broad minimum of about 2.0 MeV centered at about 21 MeV. It then rises sharply to an average neutron energy of 3.1 MeV at 26 MeV, followed by a more gentle rise to a value of 3.7 MeV at about 42 MeV.

The average neutron energy for $(\gamma, 2n)$ neutrons [Fig. 2(b)] rises rapidly from the $(\gamma, 2n)$ threshold to a value of about 3.2 MeV at 20 MeV photon energy. After a narrow dip at about 21 MeV, the average neutron energy reaches its maximum value of about 3.3 MeV at 22.5 MeV, from which it decreases slowly to a very broad minimum of 1.7 MeV at about 33 MeV. It then rises slowly to about 2.3 MeV at 42 MeV photon energy.

B. Cross sections

The measured photonuclear cross sections for ^{18}O are shown in Fig. 3: Parts (a) through (e) of the figure display $\sigma(\gamma, p)$, $\sigma(\gamma, n)$, $\sigma(\gamma, 2n)$, $\sigma(\gamma, n_t) = \sigma[(\gamma, n) + (\gamma, 2n)]$, and $\sigma(\gamma, \text{tot}) = \sigma[(\gamma, n) + (\gamma, 2n) + (\gamma, p)]$, respectively. Numerous resonances are

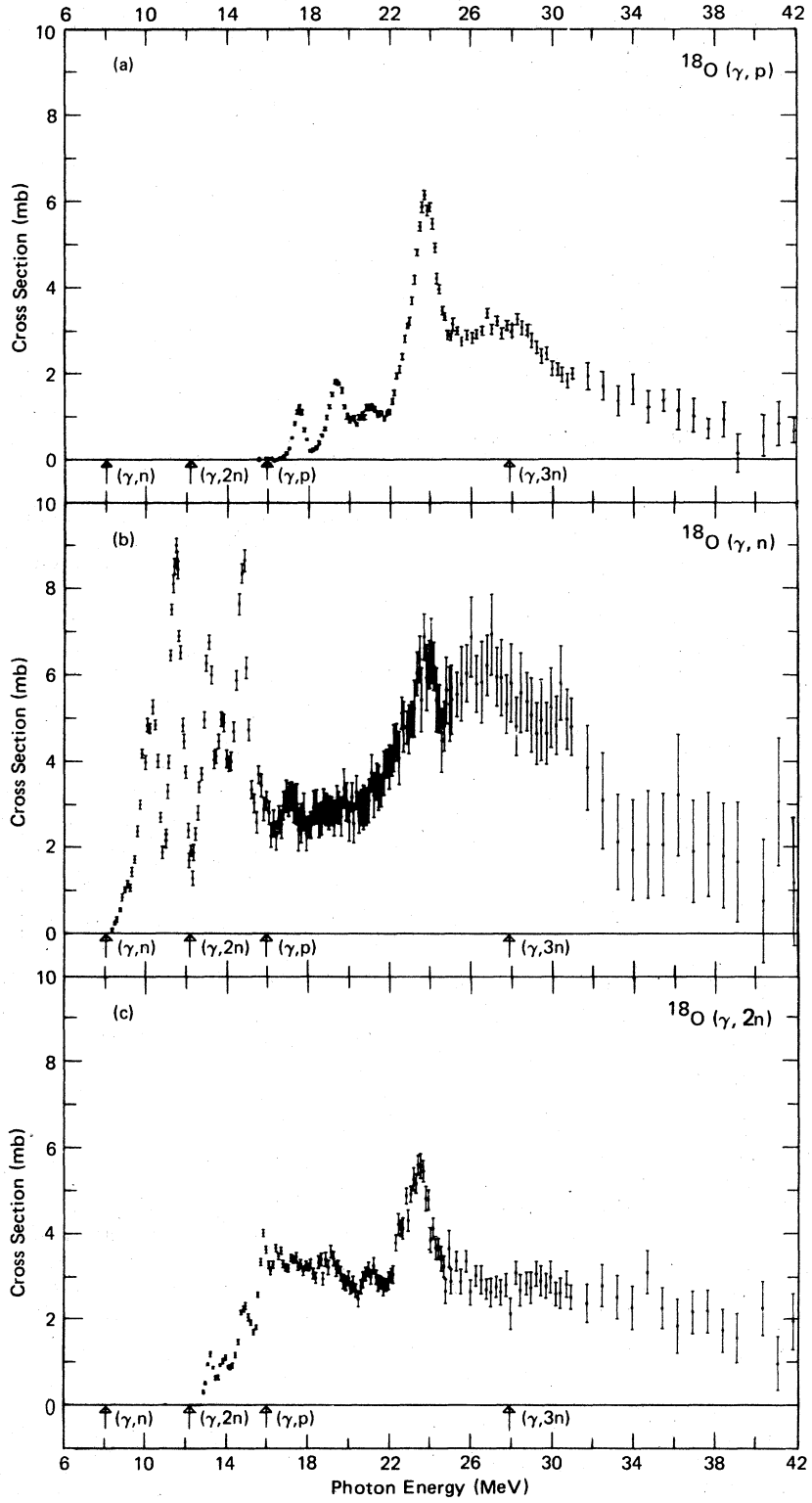

FIG. 3. Photonuclear cross section for ^{18}O: (a) $\sigma(\gamma,p)$; (b) $\sigma(\gamma,1n)=\sigma((\gamma,n)+(\gamma,np))$; (c) $\vartheta(\gamma,2n)$; (d) $\sigma(\gamma,n_t)$ $=\sigma((\gamma,1n+(\gamma,2n))$; and (e) $\sigma(\gamma,\text{tot})=\sigma((\gamma,p)+(\gamma,n_t))$.

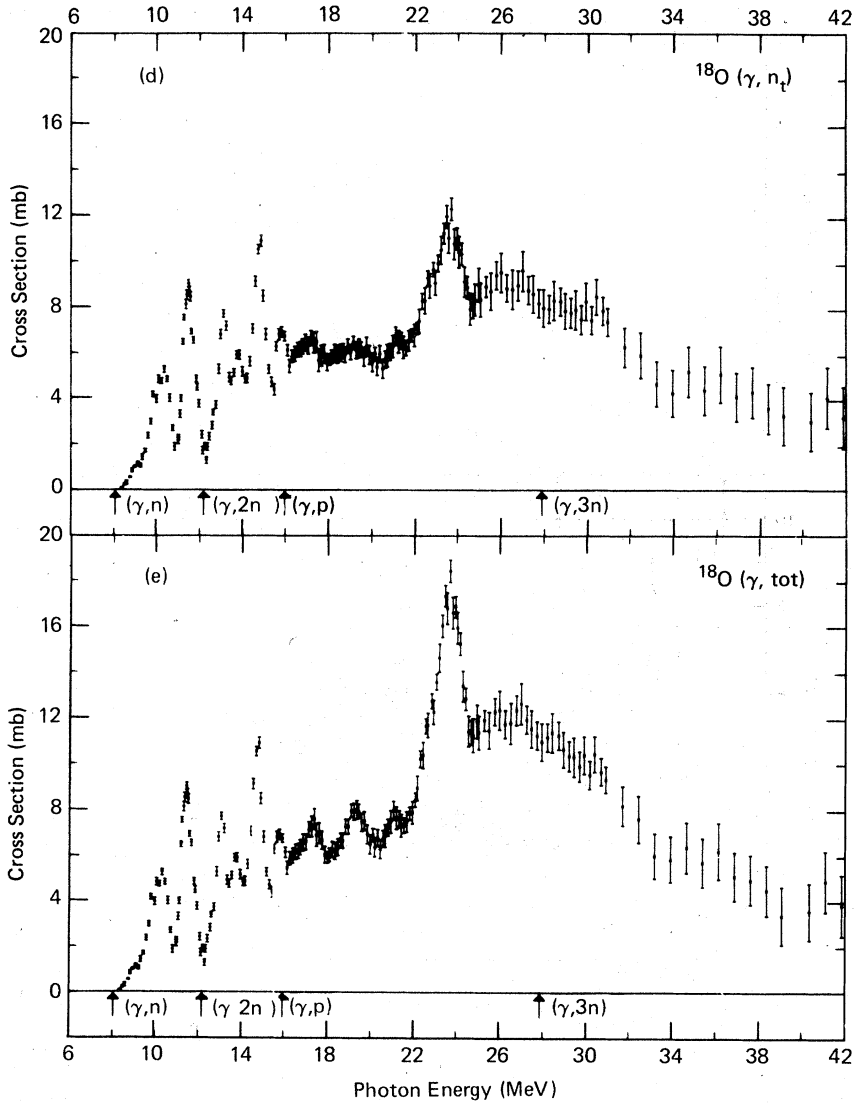

FIG. 3. (*Continued*)

seen in all of the partial cross sections, whose energies are given in Table III. The relative strengths of many resonances for the various partial cross sections varies widely; these substantial variations in the branching ratios are discussed in Sec. V.

The $^{18}O(\gamma, p)$ cross section [Fig. 3(a)] combines the results of three sets of data: (a) those taken with the large (119-g) sample, which were published in Ref. 15 (now superseded by the present results); (b) those taken with the small (35-g) sample, which extended the photon energy range from 31 to 42 MeV; and (c) those taken with the "$H_2{}^{17}O$" sample (which contained about 70 g of $H_2{}^{18}O$), since the delayed-neutron component of the data results from ^{18}O (γ, p) events alone. These data were consistent (i.e., they required no arbitrary normalization to each other), and were averaged, with proper (inverse-square) weighting, to yield the final result shown. The photoneutron results [Figs. 3(b), 3(c), and 3(d)] combine the results of the first two sets of data mentioned above. Again, no arbitrary normalization was performed.

The prominent resonances seen in the (γ, p) cross section at 17.5, 19.4, and 21.0 MeV appear only weakly or not at all in the (γ, n) channel [Fig. 3(b)], but the 23.7-MeV resonance does indeed appear strongly in, and in fact dominates, the $(\gamma, 2n)$ cross section. On the other hand, the (γ, n) channel has five distinct and prominent resonances be-

TABLE III. Energies (in MeV) of resonances observed in ^{18}O.

Present work				Ref. 13		Ref. 14	
(γ,tot)	(γ,n)	$(\gamma,2n)$	(γ,p)	(γ,n_0)	(γ,n_1)	(γ,n)	$(\gamma,2n)$
9.1	9.1						
10.3	10.3			10.2 10.4		10.3	
				11.1			
11.4	11.4			11.4 11.7	11.5	11.3	
				12.4	(12.6)		
13.1	13.1	13.2		13.1 (13.4)		13.0	
13.8	13.8	13.9				13.6	
14.7	14.7	14.8		14.7	14.6	14.5	14.5
15.8	15.7	15.8		15.6 16.7		15.6	15.6
17.3	17.1		17.5			(17.0)	
19.4		(19.1)	19.4			19.0 19.7	18.8
21.1		21.1	21.0			21.2	21.2
22.6	(22.6)	22.7	22.7			22.3	22.5
23.7	23.7	23.5	23.7			23.4	23.5
							25.6
27	27		27–28				
30	30						
36							

low the (γ,p) threshold, at 10.3, 11.4, 13.1, 13.8, and 14.7 MeV. The last three of these are evident in the $(\gamma,2n)$ cross section as well. All three of the partial cross sections measured here have substantial strength in the giant-resonance region. Unlike the situation in most other light nuclei, the $(\gamma,2n)$ cross section constitutes a significant fraction of the total cross section, and is even larger than the (γ,p) cross section. Whereas the (γ,p) and (γ,n) cross sections tail off at the higher photon energies, the $(\gamma,2n)$ cross section apparently maintains a nearly constant strength.

Since no statistically significant net triple-photoneutron events were observed in this experiment, an upper limit of approximately 0.2 mb can be placed on the $(\gamma,3n)$ cross section from its threshold near 28 MeV to the highest energy measured. Furthermore, it is reasonable to assume that all partial cross sections resulting in the emission of charged particles only [other than $\sigma(\gamma,p)$] are far smaller than the cross sections measured here. Therefore, it is highly likely that the sum of all these partial cross sections, shown in Fig. 3(e), is essentially equivalent to the total photon absorption cross section for ^{18}O.

C. Integrated cross sections

The integrated cross sections and their moments for each of the photonuclear reaction channels measured in this experiment, as well as for their sums, are given in Table IV. The integrated cross sections are $\sigma_{\text{int}}(\gamma,x) \equiv \int \sigma(\gamma,x)dE_\gamma$, and their first and second moments are $\sigma_{-1} \equiv \int \sigma E_\gamma^{-1} dE_\gamma$ and $\sigma_{-2} \equiv \int \sigma E_\gamma^{-2} dE_\gamma$, where in all cases the limits of integration extend from the threshold for the (γ,x) reaction to 41.8 MeV, the upper energy limit of this experiment. It is not surprising that the integrated strengths of the neutron channels exceed that of the proton channel because the photoneutron

TABLE IV. Integrated cross sections for ^{18}O (integrated up to 41.8 MeV).

Reaction	σ_{int} (MeV mb)	σ_{int} (sum-rule units)	σ_{-1} (mb)	σ_{-2} (mb MeV^{-1})
$^{18}O(\gamma,p)$	44.4	0.17	1.66	0.064
$^{18}O(\gamma,n)$	121.5	0.46	5.93	0.342
$^{18}O(\gamma,2n)$	76.7	0.29	3.14	0.141
$^{18}O(\gamma,n_t)$	198.3	0.74	9.08	0.483
$^{18}O(\gamma,\text{tot})$	242.6	0.91	10.73	0.547

thresholds both are considerably lower than the (γ, p) threshold (see Table I). The total integrated strength predicted by the semiclassical Thomas-Reiche-Kuhn (TRK) sum rule $\sigma_{int} = 60NZ/A$ MeV mb is 266.7 MeV mb for ^{18}O. The fractions of this value which are exhausted by the various reactions (in sum-rule units) also are given in Table IV. It is interesting that the present results, for data taken up to 41.8 MeV, exhaust nearly one TRK sum-rule unit (see Sec. V). In order to facilitate data retrieval, the integrated cross sections for the (γ, p), (γ, n), $(\gamma, 2n)$, and (γ, tot) reactions are shown in Fig. 4(a), and their first moments in Fig. 4(b), in the form of running sums plotted versus the upper photon-energy limit of integration.

V. DISCUSSION

The present work, when taken in conjunction with the work of Allan *et al.*[13] and of Kneissel *et al.*,[14] allows a very detailed account to be made of the photonuclear process in this doubly-magic-plus-2N nucleus. In view of this nuclear configuration, it would be expected that the photonuclear cross sections for ^{18}O should reflect the excitation of the two valence neutrons in addition to the effects which stem primarily from excitation of the ^{16}O core. As a consequence, it makes sense to discuss the results separately for the three energy regions below, at, and above the giant dipole resonance (GDR).

A. Region below the GDR (8 to 17 MeV)

The present photoneutron cross-section results are compared with the work of Ref. 13 in Fig. 5. In addition, Table III lists the energies of the resonances seen in Refs. 13 and 14 as well as in the present work. The present experiment yields average neutron-energy data as well; these data,

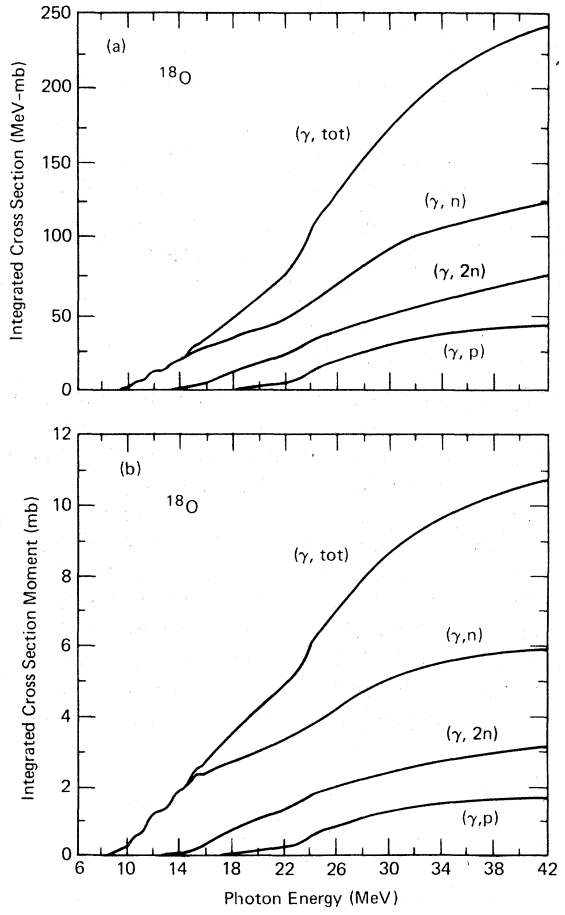

FIG. 4. Running sums of (a) the integrated cross section $\int_0^{E_\gamma} \sigma dE$ and (b) its first moment $\int_0^{E_\gamma} E^{-1} \sigma dE$. The curves in each frame are (from top to bottom) for $\sigma(\gamma, \text{tot})$, $\sigma(\gamma, n)$, $\sigma(\gamma, 2n)$, and $\sigma(\gamma, p)$.

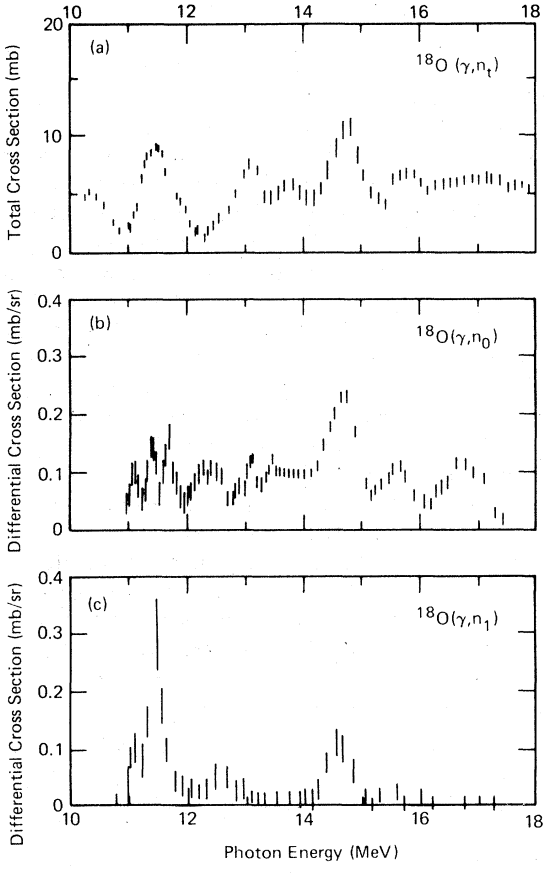

FIG. 5. The low-energy part of the photoneutron cross section from the present work compared with those of Allan *et al.* (Ref. 13): (a) present $^{18}O(\gamma, n_t)$; (b) $^{18}O(\gamma, n_0)$ from Ref. 13; and (c) $^{18}O(\gamma, n_1)$ from Ref. 13.

used in conjunction with the cross-section data, facilitate the extraction of branching ratios for each resonance. Figure 6 shows the energies of the resonances in ^{18}O and the levels in ^{17}O and ^{16}O which are relevant to the discussion below. The data for ^{16,17}O in this figure were taken from Ref. 26.

In the region below the GDR there is good agreement as far as the energies of the resonances are concerned. However, there are significant (~30%) discrepancies between the present cross-section values and those of Ref. 14 below 14 MeV. Since the photoneutron time-of-flight measurements of Ref. 13 are specific to (γ, n_0) and (γ, n_1) transitions and were performed at a single angle, direct comparison with the total cross sections is not possible.

The weak 9.1-MeV resonance, not seen elsewhere, is dominated by ground-state transitions; the evidence for this is that the average neutron energy [Fig. 2(a)] is much closer to 1 MeV than to 0.2 MeV, the neutron energies expected from ground- and first-excited-state transitions, respectively.

The broad, probably split,[13] resonance at 10.3 MeV has a peak cross section of over 5 mb. It should be noted that the peak value of Ref. 14 is 3.5 mb for this resonance. Since the average neutron energy at 10.3 MeV photon energy is about 2.0 MeV [Fig. 2(a)], there is clearly more ground-state strength (giving neutrons of 2.1 MeV) than first-excited-state strength (giving neutrons of 1.3 MeV).

The strong resonance at 11.4 MeV (with a peak cross section of 9 mb) also is seen by Kneissel *et al.*,[14] but their maximum cross-section value here is about 6 mb. By comparing their value with the values of Ref. 13 [Fig. 5] for the ground- and first-excited-state cross sections, they found that their measured cross section for this resonance was nearly exhausted by the sum of the (γ, n_0) and (γ, n_1) cross sections. However, the cross section value of 9 mb measured in this experiment greatly exceeds that sum and shows therefore that there must be appreciable strength feeding the second excited state, which is the only other level to which decay is energetically possible. Moreover, the plot of the average neutron energy shows a distinct flattening at this resonance, indicating the presence of appreciable excited-state strength.

Perhaps, however, the situation here is more complicated. Two levels are seen at 11.4 MeV in ^{14}C(α, α') data[27] and are assigned to be (2^+) and (4^+), and a strong resonance is seen at that energy in the ^{14}C(α, n) reaction[27] as well. Also, levels seen at 11.1 and 11.7 MeV in the ^{19}F$(d, ^3$He) reaction[28] are assigned to be $(0, 1, 2)^-$. Since three

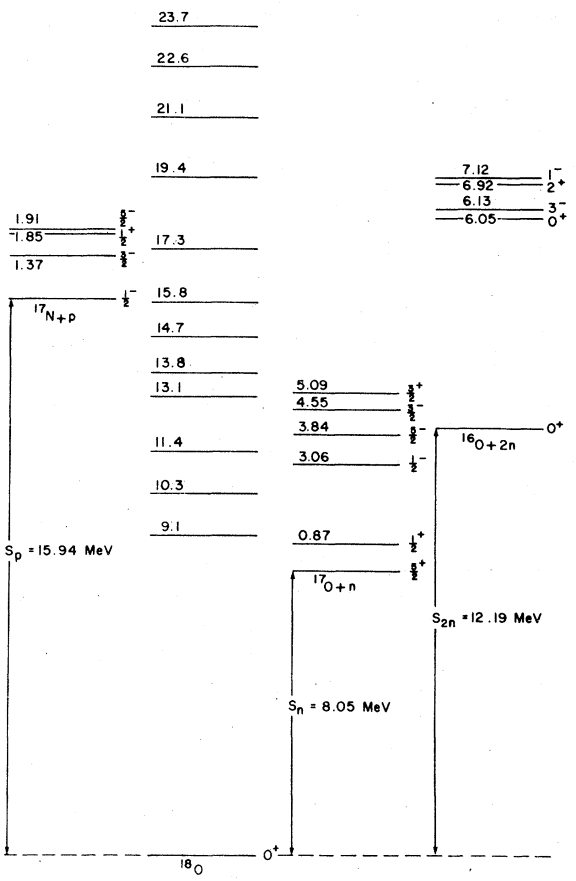

FIG. 6. The first few energy levels for ^{16}O, ^{17}O, and ^{17}N, together with the energies of the resonances in ^{18}O seen in the present experiment up to 23.7 MeV.

levels are seen in the (γ, n_0) data of Ref. 13 [and only one, at 11.5 MeV, in the (γ, n_1) data], perhaps the most likely assignments that can be made, in the light of the electromagnetic selection rules, are 1^- for the 11.1- and 11.7-MeV levels and 2^+ for the one at 11.4 MeV; the large resonance in the present data is, then, an unresolved superposition of the three.

The next two prominent resonances, which lie at 13.1 and 13.8 MeV, are seen clearly in both the (γ, n) and $(\gamma, 2n)$ cross sections, and the total photoneutron cross section at the peaks of these resonances reaches ~8 and 6 mb, respectively. Neither resonance shows strongly in the (γ, n_0) or (γ, n_1) cross sections of Ref. 13; therefore, it is likely that transitions to the negative-parity second $(\frac{1}{2}^-)$ and third $(\frac{7}{2}^-)$ excited states ($Q_2 = 11.1$ MeV, $Q_3 = 11.9$ MeV) are occuring here (see Fig. 6). The presence of these transitions probably reflects a 3p-1h component in these excited states.

The strongest resonance below the GDR, seen in

both the (γ, n) and $(\gamma, 2n)$ cross sections, lies at 14.7 MeV and reaches a peak total cross section of ~11 mb. This broad resonance also is seen prominently in the (γ, n_0) and (γ, n_1) data of Ref. 13. Once again, since the (γ, n_0) and (γ, n_1) cross sections exhaust at most about a third of the total strength of this resonance, and since the neutron energies resulting from (γ, n_0) and (γ, n_1) transitions exceed substantially the average single-photoneutron energy of 4.3 MeV [Fig. 2(a)], there must be considerable strength feeding higher-lying excited states (up to ~5 MeV) in ^{17}O. In this case, that fraction of the resonance strength (~20%) which decays via the $(\gamma, 2n)$ channel might very well pass through the $\frac{3}{2}^+$ single-particle state at 5.09 MeV. It should be noted as well that a weak level at 14.6 MeV is barely seen in the $^{19}F(d, ^3He)$ data of Ref. 28.

The resonance at 15.8 MeV, which appears much more strongly in the $(\gamma, 2n)$ than in the (γ, n) cross section, also must have a complex decay mechanism. Here, Allan *et al.*[13] report almost no evidence for any (single-photoneutron) ground- or first-excited-state strength, and the energetics of the $(\gamma, 2n)$ channel allows decays to proceed through several excited states in ^{17}O.

B. Region of the GDR (17 to 29 MeV)

In the energy region of the GDR, five major peaks occur (see Table III), at 17.3, 19.4, 21.1, 23.7, and about 27 MeV, along with a distinct shoulder at 22.6 MeV on the low-energy side of the 23.7-MeV peak, which is the most prominent peak in the ^{18}O total cross section [Fig. 3(e)]. All of these peaks are seen clearly in the (γ, p) cross section [Fig. 3(a)], in roughly the same proportions as in the total cross section. On the other hand, the 17.3- and 23.7-MeV peaks are seen only weakly in the (γ, n) cross section [Fig. 3(b)], and the major GDR strength which is manifested through this reaction channel lies at energies above 25 MeV. The peaks at 19.4 and 21.1 MeV appear in the $(\gamma, 2n)$ cross section [Fig. 3(c)], and the 22.6-MeV shoulder of the main peak at 23.7 MeV is more prominent here than in the other partial cross sections.

Comparing the present cross-section results with those of Ref. 14, it is evident that very good agreement exists throughout the energy range from 17 to 25 MeV for both partial photoneutron cross sections (as well as for their sum). Above this energy, however, large discrepancies stand out between the two sets of results, which probably reflect the lack of knowledge of the average neutron energies, and consequently of the detector efficiency, in the work of Ref. 14.

The ^{18}O nucleus can be thought of as a pair of valence neutrons bound to the doubly magic ^{16}O core. In this view, the GDR could be expected to resemble closely that for ^{16}O, since the effects of the valence neutrons most probably would be manifested in the energy region below the GDR. In particular, if the core were not affected strongly by the presence of the two extra-core neutrons, it might be expected that a strong similarity would exist between the present (γ, p) cross section and that for the ^{16}O nucleus. But, as can be seen from the comparison of these two (γ, p) cross sections, shown in Fig. 7(a), such is not the case. Whereas the ^{18}O (γ, p) cross section is dominated by two major peaks at 23.7 and 27–28 MeV, the ^{16}O (γ, p) cross section contains four narrower and more tightly clustered peaks at 22.3, 23.1, 24.2, and 25.2 MeV. The similarities and differences between these two photoproton cross sections have been discussed at length in Ref. 15. [The cross-section curves for ^{16}O shown in Fig. 7 are composites constructed from various results in the literature. Values for the ^{16}O (γ, p_0) cross section have been taken from Refs. 29 and 30, normalized to the mean of several other published measurements; for ^{16}O $(\gamma, p_{t>0})$, from Ref. 31; and for ^{16}O (γ, n), from Refs. 32 and 33.]

A comparison of the photoneutron branches for ^{18}O and ^{16}O, shown in Fig. 7(b), is even more dif-

TABLE V. Comparison of the integrated cross sections for ^{16}O and ^{18}O (integrated up to 29.0 MeV. The lower limit of integration for the photoneutron cross sections for ^{18}O is 16.5 MeV.)

	(γ, p)	(γ, n)	$(\gamma, 2n)$	(γ, n_t)	(γ, tot)
^{16}O:					
σ_{int} (MeV mb)	83.6	44.8	0	44.8	128.5
σ_{-1} (mb)	3.64	1.87	0	1.87	5.52
^{18}O:					
σ_{int} (MeV mb)	28.3	55.5	41.1	96.6	124.9
σ_{-1} (mb)	1.18	2.39	1.85	4.24	5.42

ficult owing mainly to the lack of as many clearly delineated peaks in the GDR region of ^{18}O as are found in that of ^{16}O. It should be noted as well that there is a strong resemblance between the photoproton and photoneutron cross sections for ^{16}O, apart from a factor of 2 in magnitude favoring the photoproton branch, but for ^{18}O, even in the GDR region rather less resemblance is found, and the factor of 2 (or more) in the branching goes the other way.

However, a comparison of the total cross sections for ^{16}O and ^{18}O, shown in Fig. 7(c), shows that there is rather greater similarity between them than the comparisons of the partial cross sections might have led one to expect. Presumably, this results from compensating effects, such as relative threshold differences and competition between the reaction channels.

Another way of comparing the GDR cross sections for ^{16}O and ^{18}O is to examine the appropriate integrated cross sections. Table V gives these integrated cross sections and their first moments integrated up to 29.0 MeV; for the photoneutron cross sections for ^{18}O, the lower limit of integration is 16.5 MeV (in order to remove from consideration, insofar as this is possible, the effect of the valence neutrons in the pygmy-resonance region), while for the other reaction channels the integrations are carried out from their respective thresholds. It now is clear that the compensation mentioned above is almost complete.

The resonance at 21.1 MeV in ^{18}O, seen in the (γ, p) and $(\gamma, 2n)$ cross sections, is of particular interest. As will be seen below, this resonance can be identified as $T_<$; moreover, the average energy of neutrons from the $(\gamma, 2n)$ reaction is sharply reduced at this resonance [Fig. 3(b)]. This low average energy eliminates the possibility that the two-neutron decay (whether simultaneous or sequential through an excited state in ^{17}O) goes directly to the ground state of the residual ^{16}O nucleus (see Fig. 6). Also, energy considerations favor the 6-MeV doublet in ^{16}O over the 7-MeV doublet (no higher-energy states are energetically possible), and angular-momentum considerations favor the 0^+ member of the 6-MeV doublet over its 3^- member. Therefore, it might very well be the case that the configuration of the 21.1-MeV resonance in ^{18}O is related in a simple way to that of the highly deformed 0^+ state at 6.05 MeV in ^{16}O. Since this state is known to have a large 4p-4h component, then so should the 21.1-MeV resonance; therefore, one would expect a corresponding peak in the ^{18}O (γ, α) cross sections, since the $T_<$ assignment of this resonance would allow this reaction to proceed to the ground or to other low-lying $T = 1$ states in ^{14}C.

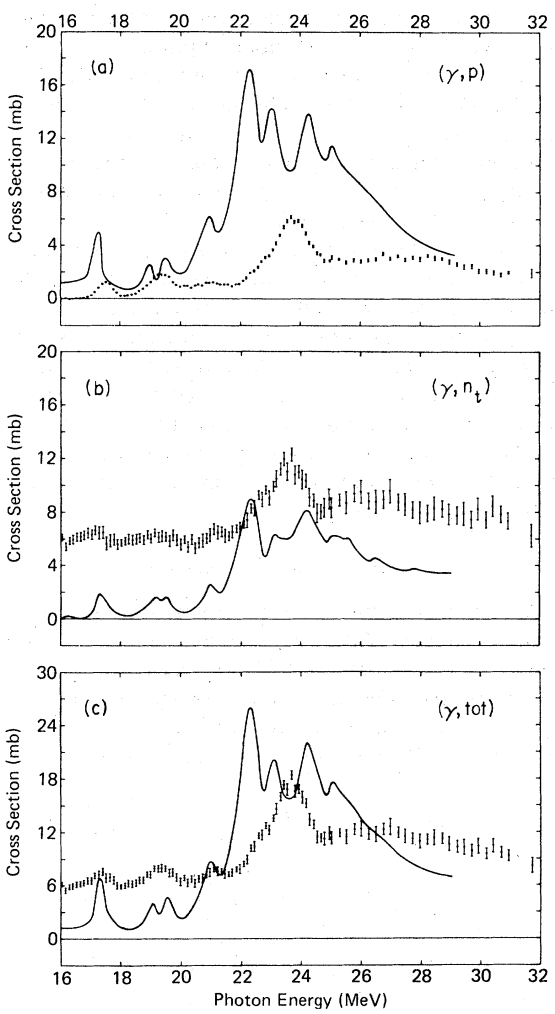

FIG. 7. Comparison of the photonuclear cross sections for ^{16}O (solid lines) and ^{18}O (data points): (a) $\sigma(\gamma, p)$; (b) $\sigma(\gamma, n_t)$. and (c) $\sigma(\gamma, \text{tot})$.

C. Region above the GDR (29 to 42 MeV)

In the region above the GDR all the partial cross sections for ^{18}O tail off but still remain substantial. In fact, the integrated (γ, tot) cross section between 29 and 42 MeV is about one-third of the value integrated from threshold to 42 MeV. It is hard to predict the amount of additional dipole strength which lies above 42 MeV. Since the $E1$ strength integrated up to the pion threshold is a subject of great current interest, a measurement of the total photon absorption cross section up to the pion threshold for this interesting non-self-conjugate nucleus would be very valuable, with the present results constituting a constraint on the accuracy of such a measurement.

In both the (γ, n) and (γ, tot) cross sections, there

is some evidence for a weak but broad resonance at about 30 MeV. No obvious explanation for such a resonance is apparent, but several particle-hole configurations in ^{18}O might be candidates, and similar weak structure is seen in $^{16}O(\gamma, n)$ cross-section results which encompass this energy,[34,35] as well as in the ^{12}C and ^{13}C photoneutron data of Refs. 36 and 1, respectively.

Although the statistical precision of the present measurement of the partial cross sections in the energy region above 30 MeV prevent the discernment of any other particular features, an examination of the total cross section of Fig. 3(e) yields evidence for a resonance centered at about 36 MeV. This might very well signal the excitation of the $1s$ nucleons in the core, as has been suggested as well in the measurements on ^{12}C (Ref. 36) and ^{13}C (Ref. 1).

D. Isospin considerations

An attempt is made here to assign a definite isospin to each observed resonance in the photonuclear cross sections for ^{18}O, in order to determine the gross distribution of isospin strength in this nucleus, including the ratio of $T_<$ and $T_>$ strengths and their splitting in energy, which then can be compared with theoretical predictions. The following analysis, therefore, assumes good isospin.

Figure 8 shows the states available via $E1$ photoexcitation and points out the nucleon decay channels which are *not* allowed by the isospin selection rule. Also shown are the energies of the first $T_>$ states known in each of the possible daughter nuclei. Below 19.1 MeV $T_>=2$ states cannot decay via single neutron emission because decay to $T=\frac{1}{2}$ states in ^{17}O is not allowed. Similarly, below 25.0 MeV, the $(\gamma, 2n)$ reaction can proceed from $T_<$ states only in ^{18}O (in the absence of isospin mixing in intermediate states in ^{17}O). The energy of the first $T=\frac{5}{2}$ state in ^{17}N is unknown, but proton decay from both $T_>$ and $T_<$ states is possible above the proton emission theshold.

Assuming that emitted neutrons and protons have equal penetrabilities, relationships have been derived by Bangert *et al.*[37] for the relative cross sections for (γ, p) and (γ, n) reactions. For decay to $T=T_0+\frac{1}{2}$ states in the daughter nucleus, where T_0 is the ground-state isospin of the target nucleus,

$$\frac{\sigma_>(\gamma, p)}{\sigma_>(\gamma, n)} = \frac{1}{2T_0+1} \tag{1}$$

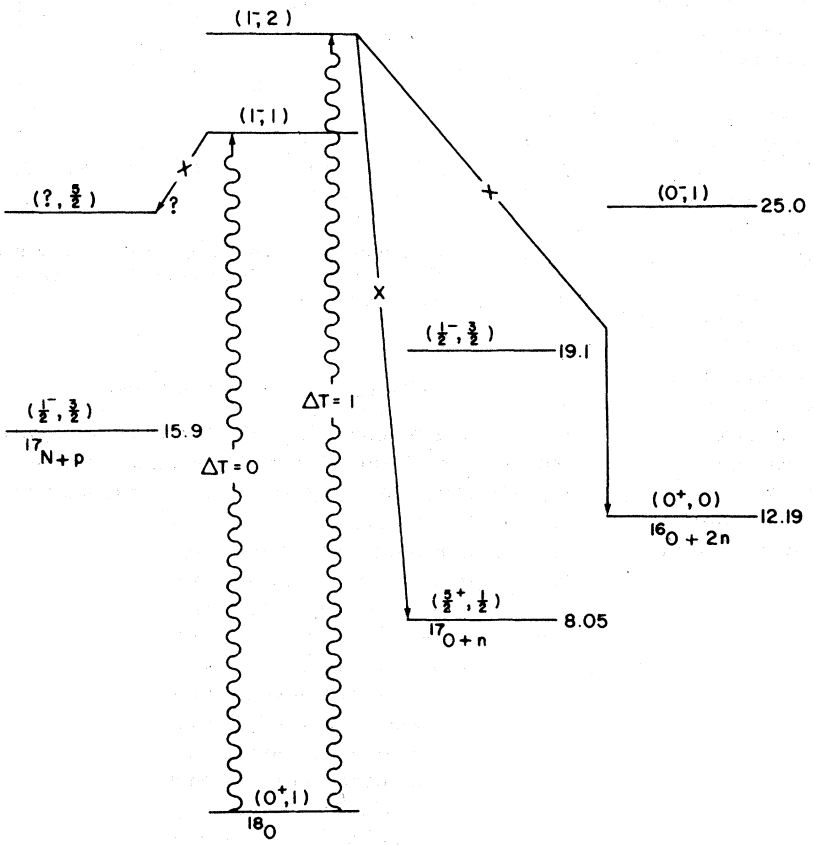

FIG. 8. Isospin energy-level diagram, showing the energies of the first $T_>$ states for ^{17}N, ^{17}O, and ^{16}O. Also shown are the nucleon decays forbidden by the isospin selection rule.

and

$$\frac{\sigma_<(\gamma,p)}{\sigma_<(\gamma,n)} = 2T_0 + 1 . \qquad (2)$$

These relations show that for decay to $T=\frac{3}{2}$ states the neutron channels will be enhanced in the $T_>$ case and proton channels in the $T_<$ case. It is noted that proton decay also can occur to $T=\frac{5}{2}$ states from a $T_>$ resonance, while neutron decay can occur to $T=\frac{1}{2}$ states from a $T_<$ resonance.

The experimental data now can be examined. For single-photoneutron reactions in ^{18}O, the average neutron energy [Fig. 2(a)] falls sharply between 16.5 and 18.5 MeV, *before* neutron decay from $T_>$ states is energetically possible. The fact that $T_>$ states cannot appear below at least 19.1 MeV in $\sigma(\gamma,n)$ supports the idea that neutrons are being promoted from the core in this energy region.

The most prominent features in the total cross section for the GDR energy region are a peak at 23.7 MeV and a broad resonance centered at about 27 MeV. The former peak is seen very strongly in $\sigma(\gamma,2n)$ and relatively weakly in $\sigma(\gamma,n)$, whereas the latter is seen very strongly in $\sigma(\gamma,n)$ and hardly at all in $\sigma(\gamma,2n)$. The absence of appreciable nel compared to the (γ,n) is in approximate agreement with Eq. (2), which predicts $\sigma_<(\gamma,p)/\sigma_<(\gamma,n) = 3$ for ^{18}O. The broad resonance at ~27 MeV might be the $T_>$ component of the GDR. The relative sizes of $\sigma(\gamma,p)$ and $\sigma(\gamma,n)$ here are in approximate agreement with Eq. (1), which predicts $\sigma_>(\gamma,p)/\sigma_>(\gamma,n)=\frac{1}{3}$. Thus, the relative strengths of all the partial cross sections establish the isospin assignments of the two major peaks, at 23.7 and 27 MeV, to be $T=1$ and $T=2$, respectively.

The other three prominent resonances in the (γ,p) channel, at 17.3, 19.4, and 21.1 MeV can be assigned isospin values of 2, 2, and 1, respectively, on the following bases. For the 17.3-MeV resonance, neutron decay from a $T_>$ state is not allowed energetically. Since this resonance is not seen strongly in either photoneutron channel, it can be assigned to have $T=2$. The same argument applies for the 19.4-MeV peak, although it is just possible to reach the first $T=\frac{3}{2}$ state in ^{17}O at 19.1 MeV. If penetrabilities were equal, Eq. (1) would predict an enhancement of a factor of three for the neutron over the proton channel for a $T_>$ decay. However, the ratio of neutron to proton penetrabilities is ~0.2 for $l=0$ neutrons (and less for higher l values), thus offsetting the result predicted by Eq. (1). For the resonance at 21.1 MeV, its $(\gamma,2n)$ decay from the 27-MeV peak implies little, if any, isospin mixing in intermediate states of ^{17}O up to 19 MeV, and also argues a favor of a $T_>$ assignment for this resonance. Since the peak at 23.7 MeV is seen strongly in $\sigma(\gamma,2n)$, and since it now can be said that there is no appreciable isospin mixing in ^{17}O, this resonance can be assigned as $T_<$ on the basis that its energy is below 25.0 MeV (which is equivalent to 17 MeV in ^{17}O). The relative size of this peak as seen in the (γ,p) chan- appearance in $\sigma(\gamma,2n)$ argues against a $T_>$ assignment. This resonance does not appear in $\sigma(\gamma,n)$, consistent with Eq. (2), which predicts an enhancement of $\sigma(\gamma,p)$ by a factor of 3 over $\sigma(\gamma,n)$ for $T_<$ resonances.

In order to compare the present data with isospin sum rules, it is necessary to separate the two components. This cannot be done in the present case without ambiguity, but reasonable assumptions allow separation of the components across the region of the GDR. Defining $\sigma^p_< + \sigma^p_> \equiv \sigma^p$ and $\sigma^n_< + \sigma^n_> \equiv \sigma^n$, Eqs. (1) and (2) yield $\sigma^p_< = 3\sigma^n_<$ and $\sigma^p_> = \sigma^n_>/3$. For $\sigma(\gamma,n)$ and $\sigma(\gamma,p)$ below 20 MeV, the strength is assumed to be $T_<$ except for the two $T_>$ resonances at 17.3 and 19.4 MeV. The $(\gamma,2n)$ strength is assumed to be all $T_<$ below 27 MeV; above 27 MeV, $T_<$ and $T_>$ assignments for the $(\gamma,2n)$ strength are made in the same proportion as given by the sum of those for the (γ,n) and (γ,p) channels. Solution of these simultaneous equations then gives the $T_<$ and $T_>$ components for the neutron and proton channels. The resulting "pure" isospin cross sections $\sigma_<$ and $\sigma_>$, given by $\sigma_< \equiv \sigma^p_< + \sigma^n_< + \sigma^{2n}_<$ and $\sigma_> \equiv \sigma^p_> + \sigma^{2n}_>$, are shown in Fig. 9. The integrated cross sections are given in Table VI.

A sum rule given by Hayward *et al.*[38] predicts the relative strengths of the two isospin components to be

$$\frac{\sigma_{-1}(T+1)}{\sigma_{-1}} = \frac{1}{T+1}\left[1 - \frac{1.97\langle R^2\rangle}{A^{4/3}}(1-\delta)\right], \qquad (3)$$

where $\langle R^2\rangle^{1/2}$ is the rms charge radius and $\delta = (2T-1)A^{2/3}/3NZ$ is small. The use of the empirical value measured by Miska *et al.*[39] of $\langle R^2\rangle^{1/2} = 2.794$ fm leads to $\sigma_{-1}(T=2)/\sigma_{-1} = 0.342$, so that $\sigma_{-1}(T=2)/\sigma_{-1}(T=1) = 0.52$. The present measured value for this ratio, 0.64 ± 0.13, is in reasonable agreement with the sum-rule prediction.

It is expected that the $T_<$ and $T_>$ components of the GDR will be separated by an energy given by Akyüz and Fallieros[40] to be

$$\Delta E = E_{T+1} - E_T = \frac{U(T+1)}{A} , \qquad (4)$$

where the dipole symmetry energy U is about 60 MeV, giving $\Delta E \simeq 6.7$ MeV. Leonardi and Lipparini[41] predict $U \sim 40$ MeV for ^{18}O, thus giving $\Delta E \sim 4.4$ MeV. If the energy of the $T_<$ strength is chosen to coincide with the major peak in the $T_<$ cross section [Fig. 9(b)] at 23.7 MeV and that of

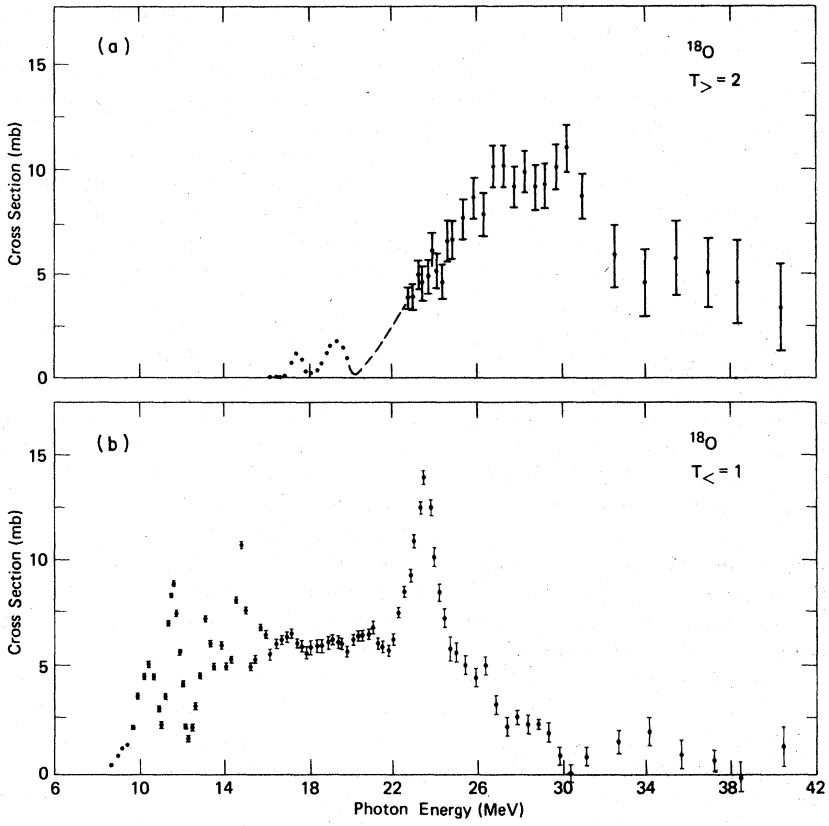

FIG. 9. Isospin components of the ^{18}O photoabsorption cross section, derived as described in the text: (a)$\sigma_>$, the $T_>$ = 2 cross section; and (b) $\sigma_<$, the $T_<$ = 1 cross section. The data points have been average in pairs for purposes of this of this analysis. The dashed line represents estimated values.

the $T_>$ strength to be the centroid of the broad maximum in the $T_>$ cross section [Fig. 9(a)] at ~29 MeV, then the present measurement yields a value for ΔE of ~5.3 MeV, lying between and in reasonable agreement with these theoretical predictions.

VI. SUMMARY AND CONCLUSIONS

All the major photonuclear cross sections for ^{18}O were measured from threshold to 42 MeV with monoenergetic photons of good resolution. These cross sections, $\sigma(\gamma, p)$, $\sigma(\gamma, n)$, $\sigma(\gamma, 2n)$, $\sigma(\gamma, n_t)$, and $\sigma(\gamma, \text{tot})$, were measured simultaneously and independently, using the same beam, the same samples, and the same detector, thus effecting an internal consistency unique for such photonuclear measurements to date. The average energies of the emitted photoneutrons were measured simultaneously as well, for both the $(\gamma, 1n)$ and $(\gamma, 2n)$ reaction channels. Integrated cross sections and their moments for all the reaction channels are presented along with the cross-section data.

Much structure is seen in the cross sections. For several of the resonances seen in the pygmy-resonance region below 17 MeV, the cross-section and photoneutron-energy data acquired here were combined with the (γ, n_0) and (γ, n_1) data of Allan *et al.*[13] to extract nuclear spectroscopic information that shows a complex behavior for the decay of the resonances in this energy region. In particular, the substantial neutron decay to the low-lying negative-parity states in ^{17}O shows that states in the pygmy-resonance region of ^{18}O contain appreciable 3p-1h components.

For the giant-resonance region, the branching of the various resonances into their decay modes also shows a complex pattern. Using this branch-

TABLE VI. Integrated cross sections for the separated isospin components.

Isospin	σ_{int} (MeV mb)	σ_{-1} (mb)
$T_<=1$	122.2	6.52
$T_>=2$	120.4	4.20

ing-ratio information along with the average photoneutron energies, isospin assignments were made for all the resonances, and the resulting distributions of $T_<$ and $T_>$ strength shows good agreement with predictions of theoretical sum-rule and isospin-splitting calculations.

Evidence for weak but broad resonances at about 30 and 36 MeV might indicate the presence of high-energy particle-hole states. Similar evidence has been seen as well for ^{16}O and for the carbon isotopes.

Comparisons of the ^{18}O cross sections were made with the corresponding cross sections for ^{16}O, illustrating the differences between these two nuclei, which go beyond the expectations based upon a picture of the ^{18}O nucleus as an ^{16}O core which is only weakly coupled to and perturbed by two valence neutrons.

Finally, the integrated (γ, tot) cross section for ^{18}O as measured here exhausts nearly one TRK sum-rule unit up to 42 MeV. A total cross-section measurement extending to the meson threshold, but constrained by the present results at the lower energies, would constitute a valuable addition to our knowledge of this interesting light non-self-conjugate nucleus.

Preliminary reports of this work appeared as Refs. 39 and 40. The data in the present paper supersede as well the preliminary data presented in Lawrence Livermore Laboratory Report No. UCRL-78482, 1976 (unpublished).

ACKNOWLEDGMENTS

We acknowledge with thanks the help of the operations and support staff of the LLL linac. Work performed under the auspices of the U. S. Department of Energy under Contract No. W-7405-ENG-48 and supported in part by the National Research Council of Canada.

*Permanent address: Department of Physics, University of Toronto, Toronto, Ontario, Canada M5S 1A7.
†Permanent address: Department of Physics, Trent University, Peterborough, Ontario, Canada K9J 7B8.

[1]J. W. Jury, B. L. Berman, D. D. Faul, P. Meyer, K. G. McNeil, and J. G. Woodworth, following paper, Phys. Rev. C 19, 1684 (1979).
[2]R. G. Johnson, K. G. McNeill, J. G. Woodworth, J. W. Jury, and B. L. Berman, Phys. Rev. C (to be published).
[3]A. H. Wapstra and K. Bos, At. Data Nuclear Data Tables 19, 215 (1977).
[4]S. C. Fultz, R. A. Alvarez, B. L. Berman, M. A. Kelly, D. R. Lasher, T. W. Phillips, and J. McElhinney, Phys. Rev. C 4, 149 (1971).
[5]H. Fuchs, Z. Phys. 171, 416 (1963).
[6]S. F. Mughabghab and W. E. Stephens, Phys. Rev. 133, B660 (1964).
[7]W. E. Stephens, J. Halpern, and R. Sher, Phys. Rev. 82, 511 (1951).
[8]R. Montalbetti and L. Katz, Can. J. Phys. 31, 798 (1953).
[9]M. M. Dorosh, N. P. Mazyukevich, and V. A. Shkoda-Ulyanov, Ukr. Fiz. Zh. 17, 847 (1972).
[10]R. Kosiek, K. Schlüpmann, H. W. Siebert, and R. Wendling, Z. Phys. 179, 9 (1964).
[11]W. Hofmann, R. Kosiek, G. Kraft, and R. Mundhenke, Z. Phys. 225, 303 (1969).
[12]G. J. Vanpraet, Phys. Lett. 17, 120 (1965).
[13]J. D. Allan, J. W. Jury, R. G. Johnson, K. G. McNeill. J. G. Woodworth, and Y. S. Horowitz, Can. J. Phys. 53, 786 (1975).
[14]U. Kneissl, K. H. Leister, H. O. Neidel, and A. Weller, Nucl. Phys. A272, 125 (1976).
[15]B. L. Berman, D. D. Faul, R. A. Alvarez, and P. Meyer, Phys. Rev. Lett. 36, 1441 (1976).
[16]B. L. Berman, J. T. Caldwell, R. R. Harvey, M. A. Kelly, R. L. Bramblett, and S. C. Fultz, Phys. Rev. 162, 1098 (1967).
[17]B. L. Berman, R. L. Bramblett, J. T. Caldwell, H. S. Davis, M. A. Kelly, and S. C. Fultz, Phys. Rev. 177, 1745 (1969).
[18]S. C. Fultz, R. A. Alvarez, B. L. Berman, and P. Meyer, Phys. Rev. C 10, 608 (1974).
[19]B. L. Berman, in *Nuclear Spectroscopy and Reactions*, edited by J. Cerny (Academic, New York, 1974), Chap. VIII A p. 377.
[20]B. L. Berman and S. C. Fultz, Lawrence Livermore Laboratory Report No. UCRL-75383, 1974 (unpublished).
[21]B. L. Berman and S. C. Fultz, Rev. Mod. Phys. 47, 713 (1975).
[22]J. G. Woodworth, K. G. McNeill, J. W. Jury, R. A. Alvarez, B. L. Berman, D. D. Faul, and P. Meyer, LLL Report No. UCRL-77471, 1978 (unpublished).
[23]E. Plechaty and J. Kimlinger, Lawrence Livermore Laboratory Report No. UCRL-50400, Vol. 14, 1976 (unpublished).
[24]H. Ohm, W. Rudolf, and K. -L. Kratz, Nucl. Phys. A274, 45 (1976).
[25]G. W. Grodstein, National Bureau of Standards Circular No. 583, 1957 (unpublished).
[26]F. Ajzenberg-Selove, Nucl. Phys. A281, 1 (1977).
[27]G. L. Morgan, D. R. Tilley, G. E. Mitchell, R. A. Hilko, and N. R. Roberson, Nucl. Phys. A148, 480 (1970).
[28]G. Th. Kaschl, G. J. Wagner, G. Mairle, U. Schmidt-Rohr, and P. Turek, Nucl. Phys. A155, 417 (1970).
[29]R. C. Morrison, thesis, Yale University, 1965 (unpublished).
[30]J. E. E. Baglin and M. N. Thompson, Nucl. Phys. A138, 73 (1969).
[31]J. T. Caldwell, Ph.D thesis, Lawrence Livermore Laboratory Report No. UCRL-50287, 1967 (unpublished).
[32]R. L. Bramblett, J. T. Caldwell, R. R. Harvey, and S. C. Fultz, Phys. Rev. 133, B869 (1964).
[33]J. T. Caldwell, R. L. Bramblett, B. L. Berman, R. R. Harvey, and S. C. Fultz, Phys. Rev. Lett. 15, 976 (1965).
[34]A. Veyssière, H. Beil, R. Bergère, P. Carlos, A. Le-

prêtre, and A. de Miniac, Nucl. Phys. A227, 513 (1974).
[35]U. Kneissl, E. A. Koop, G. Kuhl, K. H. Leister, and A. Weller, Nucl. Instrum. Methods 127, 1 (1975).
[36]S. C. Fultz, J. T. Caldwell, B. L. Berman, R. L. Bram Bramblett, and R. R. Harvey, Phys. Rev. 143, 790 (1966).
[37]K. Bangert, U. E. P. Berg, G. Junghans, R. Stock, K. Wienhard, and H. Wolf, Nucl. Phys. A261, 149 (1976).
[38]E. Hayward, B. F. Gibson, and J. S. O'Connell, Phys. Rev. C 5, 846 (1972).
[39]D. D. Faul *et al.*, Bull. Am. Phys. Soc. 21, 68 (1976).
[40]B. L. Berman, D. D. Faul, R. A. Alvarez, and P. Meyer, Phys. Rev. Lett. 36, 1441 (1976).
[39]H. Miska, B. Norum, M. V. Hynes, W. Bertozzi, S. Kowalski, F. N. Rad, C. P. Sargent, T. Sasanuma, and B. L. Berman, Phys. Lett. (to be published).
[40]R. O. Akyüz and S. Fallieros, Phys. Rev. Lett. 27, 1016 (1971).
[41]R. Leonardi and E. Lipparini, Phys. Rev. C 11, 2073 (1975).